

# Unravelling the Acoustic and Thermal Responses of Perfluorocarbon Liquid Droplets Stabilized with Cellulose Nanofibers

Morteza Ghorbani,<sup>†,‡</sup> Karl Olofsson,<sup>§</sup> Jan-Willem Benjamins,<sup>||</sup> Ksenia Loskutova,<sup>†</sup> Thomas Paulraj,<sup>⊥,¶</sup> Martin Wiklund,<sup>§</sup> Dmitry Grishenkov,<sup>†</sup> and Anna J. Svagan<sup>\*,†,¶</sup>

<sup>†</sup>Department of Biomedical Engineering and Health Systems, KTH Royal Institute of Technology, SE-100 44 Stockholm, Sweden

<sup>‡</sup>Mechatronics Engineering Program, Faculty of Engineering and Natural Science, Sabanci University, Istanbul 34956, Turkey

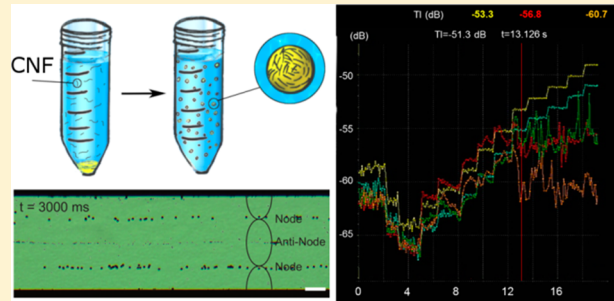
<sup>§</sup>Department of Applied Physics, KTH Royal Institute of Technology SE-100 44 Stockholm, Sweden

<sup>||</sup>Research Institute of Sweden (RISE), Chemistry, Materials and Surfaces, Box 5607, SE-114 86 Stockholm, Sweden

<sup>⊥</sup>Department of Fiber and Polymer Technology, KTH Royal Institute of Technology, SE-100 44 Stockholm, Sweden

## Supporting Information

**ABSTRACT:** The attractive colloidal and physicochemical properties of cellulose nanofibers (CNFs) at interfaces have recently been exploited in the facile production of a number of environmentally benign materials, e.g. foams, emulsions, and capsules. Herein, these unique properties are exploited in a new type of CNF-stabilized perfluoropentane droplets produced via a straightforward and simple mixing protocol. Droplets with a comparatively narrow size distribution (ca. 1–5  $\mu\text{m}$  in diameter) were fabricated, and their potential in the acoustic droplet vaporization process was evaluated. For this, the particle-stabilized droplets were assessed in three independent experimental examinations, namely temperature, acoustic, and ultrasonic standing wave tests. During the acoustic droplet vaporization (ADV) process, droplets were converted to gas-filled microbubbles, offering enhanced visualization by ultrasound. The acoustic pressure threshold of about 0.62 MPa was identified for the cellulose-stabilized droplets. A phase transition temperature of about 22 °C was observed, at which a significant fraction of larger droplets (above ca. 3  $\mu\text{m}$  in diameter) were converted into bubbles, whereas a large part of the population of smaller droplets were stable up to higher temperatures (temperatures up to 45 °C tested). Moreover, under ultrasound standing wave conditions, droplets were relocated to antinodes demonstrating the behavior associated with the negative contrast particles. The combined results make the CNF-stabilized droplets interesting in cell-droplet interaction experiments and ultrasound imaging.



## 1. INTRODUCTION

Studies on acoustic droplet vaporization (ADV), also denoted “phase-shift emulsion” and “ultrasonic droplet vaporization”, have been broadened in recent years due to its potential in medical applications such as embolotherapy,<sup>1,2</sup> targeted drug delivery<sup>3</sup> and high intensity focused ultrasound (HIFU) enhancement.<sup>4</sup> ADV is a progressive cycle of droplet vaporization, bubble formation, and bubble rupture. It has potential for meeting echogenicity enhancement needs with localized noninvasive energy exposure, which could improve imaging<sup>5</sup> and possibly enable diagnostic imaging combined with critical medical treatment.<sup>6</sup> The recent attempts to develop the ADV concept have widened the use of ultrasound agitated microbubbles to embolotherapy, which includes cancer and tumor treatments. Apart from the dependency on the characteristics of applied ultrasound waves, the treatment can be further enhanced by ADV-induced droplet size increase, which modifies the surrounding fluid properties.<sup>7</sup> Additionally, the droplet-to-bubble transition can be combined with controlled ultrasound excitation frequency (both in space

and time), which affects the location of the initial nucleation generation.<sup>8</sup> Seda et al.<sup>9</sup> reported an improved treatment of vascularized tumors by manipulating the pulse repetition frequency (PRF). They showed that vaporization at higher PRF results in occluding the vessels and therefore enhances the local therapeutic efficiency. Moreover, the medical diagnosis and therapy for the extravascular ultrasound imaging can be further enhanced with the knowledge of the phase shift threshold.<sup>10</sup> Ho et al. demonstrated that ultrasound-induced nanodroplets, which in this case possessed a long lifetime, can provide a persistent treatment in tumor therapy.<sup>11</sup> The long lifetime of nanodroplets, in combination with ADV induced vascular disruption, enabled the drug to penetrate and affect a larger tumor volume.

Droplets suitable for ADV are typically formed by encapsulating a liquid with a boiling point near or below

Received: July 9, 2019

Revised: September 10, 2019

Published: September 24, 2019

body temperature. Fluorocarbons are good candidates because they have relatively low toxicity.<sup>12</sup> Fluorocarbon droplets are typically emulsified using lipids or proteins, such as albumin.<sup>13,14</sup> To further increase shelf life, stability, and address clinical compatibility, other emulsifying agents have been proposed. As an example, Rapoport et al. prepared robust block copolymer stabilized perfluorocarbon (PFP) nanoemulsions to decrease PFP droplet instability during the storage and phase transition.<sup>15</sup> These PFP droplets were utilized in cancer cell treatment. Similarly, Aliabouzar et al. investigated lipid-coated PFP droplets and found that the excitation threshold pressure, required for phase shift, occurred at higher magnitudes when exposing droplets to higher frequencies.<sup>16</sup> In another study, Capece et al. used dextran and hyaluronic acid (HA) to prepare capsules with perfluorocarbon (PFC) cores which were both biocompatible and biodegradable.<sup>17</sup> A 2-fold rise and recovery in the mean diameter was reported during ultrasound exposure (transition to microbubbles) and dissipation, respectively. The authors claimed that these polymer-shelled microbubbles (MBs) could be used as theranostic devices.

A new type of PFC droplets can be obtained by using solid particles, where the oil/water (O/W) interface is stabilized via a Pickering mechanism.<sup>18,19</sup> Droplets stabilized with particles are much more stable compared to surfactant-stabilized droplets, due to the much higher desorption energies needed to remove particles from the interface.<sup>20</sup> Particle-stabilized PFC droplets should therefore demonstrate increased shelf life stability and, potentially, biological half-time.<sup>21</sup> The performance of such systems also depends on the material used in the stabilization of the PFC droplets.<sup>22</sup> Studies using stabilizing proteins<sup>23</sup> and poly(lactic-co-glycolic acid) (PLGA) particles<sup>24</sup> have been performed focusing on their potential for therapeutic applications.

In this study, cellulose nanofibers (CNF) were used as stabilizing particles of the O/W interface to create a new type of Pickering stabilized perfluorodroplets. Cellulose nanofibers have successfully been used to stabilize the O/W interface of oil-droplet consisting of, e.g., hexadecane,<sup>25–27</sup> styrene,<sup>28</sup> vegetable oil,<sup>29,30</sup> and toluene,<sup>31</sup> but there are no studies on perfluorocarbon. Also, none of the previous studies focused on acoustic and acoustophoresis applications. The advantage with CNFs with respect to acoustic applications is that micrometer-sized PFCS droplets are attained, in a comparatively narrow range, only with a very simple mixing step. This is possible due to the unique physicochemical properties of CNFs at interfaces.<sup>26</sup> The optimal size of a contrast agent is typically between 100 nm to 10  $\mu\text{m}$ , and the obtained CNF-stabilized droplets sizes fit nicely into this range. In the case of surfactants, the droplets will be more polydisperse, ranging over a few of orders of magnitude, when a similar mixing protocol is employed. For example, in the case of phospholipid-based PCF droplets, a narrow droplet size can only be achieved by running the mixture through, e.g., an extruder.

The prepared droplets were investigated in three sets of independent experiments to evaluate their potential in the acoustic droplet vaporization process. To assess temperature influence on the system, the particle-stabilized droplets were exposed to different temperatures, ranging from 4 to 45 °C, while acquiring droplet size and volume distributions. Additionally, acoustic tests were performed at different frequencies and acoustic pressures to study the phase transition

and pressure threshold value associated with ADV. Finally, the droplets were further investigated by the use of acoustophoresis, in order to evaluate their potential in such applications.

## 2. MATERIAL AND METHODS

**2.1. Materials.** Perfluoropentane (PFCS, 99%) was purchased from Apollo Scientific (City, U.K.). Bleached sulfite pulp (from Nordic Paper Seffle AB, Sweden) was used in the production of the cationic cellulose nanofibers (CNFs). The cationic CNF, which was a quaternary ammonium salt-modified CNF (1.32 wt %), was produced as described previously.<sup>32</sup> The CNFs were ca. 4 nm in width and with a length in the micrometer range. However, occasional larger nonfibrillated aggregates were also observed in the suspension.<sup>32</sup> The amount of cationic groups, obtained by conductometric titration, was 0.13 mmol per g of fiber.<sup>32</sup>

**2.2. Preparation of CNF-Stabilized PFCS Droplets.** A suspension of CNF (0.28 wt %) was prepared by diluting the stock CNF with Milli-Q water (pH of diluted CNF suspension was 9.5). The CNFs were dispersed with an ultrasonic liquid processor (Sonics Vibracell W750, U.S.). The suspension was treated at an amplitude of 90% for 180 s (using a 1/2 tip) as described previously.<sup>32</sup> The suspension was brought to room temperature, and afterward, 36 g of the (0.28 wt %) CNF suspension was mixed with 1 g of PFCS. The mixture was then processed for another 60 s at an amplitude of 80% under ice-cooling to obtain the stock suspension of CNF-stabilized PFCS droplets.

**2.3. Atomic Force Microscopy (AFM).** AFM images were obtained using a Bruker NanoScope (U.S.A) with Scanasyst-air cantilevers. The substrate was a silicon wafer, which was first thoroughly cleaned with ethanol and Milli-Q water followed by plasma cleaning for 2 min. A 0.0035 wt % CNF in Milli-Q water was prepared, and a drop was dropped on the silicon wafer. After 1 min, it was drained (with filter paper) and dried with N<sub>2</sub> and imaged immediately.

**2.4. Scanning Electron Microscopy (SEM).** A Hitachi SEM S-4800 (Japan) at an accelerating voltage of 1 kV was used. A drop on the stock suspension of CNF-stabilized PFCS droplets was dropped on top of Si wafers, allowed to dry at ambient conditions in the room, and then sputter-coated (Cressington 208HR sputter coater) with a Pt/Pd (60/40) coating (1.5 nm) prior to imaging.

**2.5. Pendant Drop–Drop/Bubble Profile Tensiometry (DPT).** Experiments were performed using a DataPhysics OCA-40 with an oscillating drop generator. The shape of the oscillating drop was monitored by a computer that records the droplet shape as a function of area change. Experiments were performed at 0.3 Hz by oscillating a droplet of CNF suspension (0.28 wt % CNF in Milli-Q water, pH 9.5) in a vial containing PFCS. The droplet was oscillated 10 times at ambient conditions ( $T = 22^\circ\text{C}$ ), and the procedure was repeated every 10 min for 1 h. As a reference, a pure water droplet was also oscillated (10 times, frequency of 0.3 Hz) in a vial containing PFCS; however, in this case, the procedure was only performed once. The complex viscoelastic modulus was calculated from

$$E = \frac{\Delta\gamma}{\frac{\Delta A}{A_0}} = E_0 + i2\pi\vartheta\eta \quad (1)$$

where  $\gamma(t)$  is the interfacial tension at time  $t$  and  $\Delta\gamma = \gamma(t) - \gamma(t=0)$ . Also,  $\Delta A = (A(t) - A_0)$ , where  $A(t)$  is the area at a specific time and  $A_0$  is the area at time = 0.  $\vartheta$  is the perturbation frequency, and  $\eta$  is the dilatational surface viscosity.  $E$  is the sum of the elastic modulus ( $E_0$ ) and the viscoelastic modulus ( $2\pi\vartheta\eta$ ). All data points are an average of two separate measurements.

**2.6. Thermal Tests.** In the thermal experiments, 200  $\mu\text{L}$  of CNF-stabilized PFCS droplets suspension was added to 1800  $\mu\text{L}$  of deionized water. The experiments were performed at three steps and were repeated four times to ensure the reproducibility. In the first step, the diluted solution was injected to the counting chamber at room temperature in order to measure the size, volume, and number

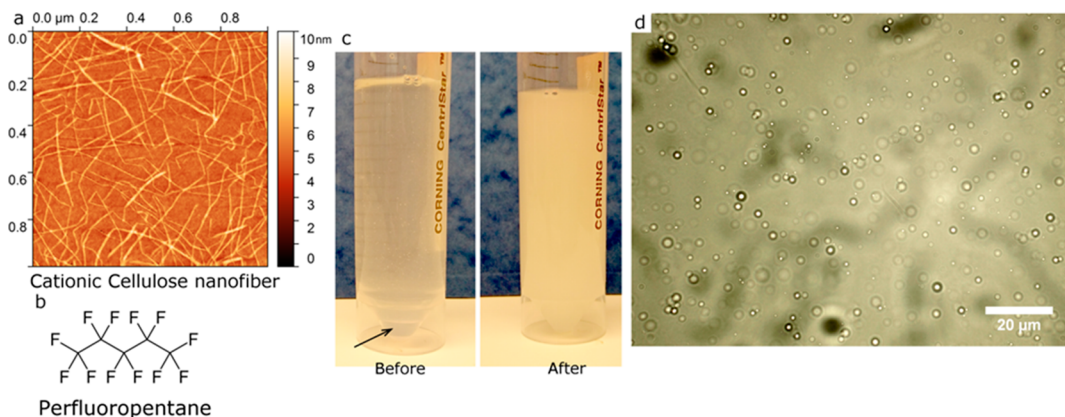


**Figure 1.** (a) AFM image of the cationic CNF used to stabilize the O/W interface of the perfluoropentane droplets. (b) Molecular structure of perfluoropentane (PFC5). (c) Suspension of CNF (0.28 wt %) and PFC prior to and after ultrasonication. The arrow points the PFC5 phase, residing on the bottom of the Falcon tube, prior to ultrasonication. (d) Optical micrographs of CNF-stabilized PFC5 droplets (imaged ca. 1 h after preparation). The sample was taken from the bulk. The suspension was diluted 10 times prior to imaging.

distribution in the sample to establish a reference case. In the second step, the temperature of the suspension was decreased to 4 °C, and the second step was finalized with assessing the droplet properties at 10 and 15 °C. In the third step, the solution was heated up to 45 °C starting from 25 °C with 5 °C increment. During heating, the solution was stirred using a magnetic stirrer. The samples were introduced in the counting chamber (with glass cover) and imaged at 20× magnification using an upright transmitted light microscope (ECLIPSE Ci-S, Nikon, Tokyo, Japan). Only the droplets that had settled or are in the vicinity of the bottom of the measurement container were investigated. This was done in order to ensure that the studied droplets were in their liquid-form. The size and volume distributions were obtained using in-house developed ImageJ script (version 1.50b, National Institutes of Health, USA). The ImageJ script eliminates objects smaller than 1 μm. For each set of experiments, corresponding to a given temperature, 32 images were taken. The presented diagrams show the normalized droplet size distribution.

**2.7. Acoustophoresis Tests.** The ultrasonic standing wave (USW)-based manipulation of droplets was performed in a straight microfluidic silicon/glass channel connected to an ultrasonic transducer. The setup is then placed in a temperature-controlled platform and is described in detail in a previous study.<sup>33</sup> In short, the microfluidic channel is a glass/silicon/glass sandwich construction where a 450 μm wide channel geometry was dry-etched straight through a 110 μm thick silicon wafer before being bonded to two glass wafers with drilled holes for fluid inlet and outlet. A 3 MHz ultrasonic piezo transducer was attached to the microfluidic chip and placed in a fluid-based temperature control platform. The fluid-based temperature control system is described in detail in a previous study.<sup>33</sup> During 3.28 MHz actuation of the piezo transducer, which corresponds to the  $\lambda$  standing wave criterion, a stationary pressure field is established across the channel width and particles suspended in the liquid-filled channel will be manipulated by ultrasonic radiation forces.<sup>34,35</sup>

To investigate the droplet behavior during ultrasonic standing wave (USW) exposure, a solution of droplets and 10 μm polystyrene beads with well-characterized material properties was prepared ( $8 \times 10^5$  beads/ml and  $2 \times 10^6$  droplets/ml in Milli-Q water). The temperature control unit was set to regulate the temperature around 15 °C to decouple possible temperature-dependent ADV from USW-induced ADV. The initial particle position manipulation after turning on the ultrasound was recorded in a microscope (Axiovert 40 CFL, Zeiss, Germany) fitted with a camera (Alpha77, Sony, Japan). To estimate the acoustic pressure amplitude in the microfluidic channel during actuation, the 10 μm polystyrene beads were segmented in the video recordings and tracked in the ImageJ plugin TrackMate.<sup>36</sup> The bead trajectories were analyzed in a MATLAB script where the position-dependent velocity was fitted against the acoustic pressure.<sup>37</sup>

**2.8. Acoustic Tests.** The acoustic tests were performed on a Vivid E9 ultrasound scanner (GE Healthcare, Wauwatosa, WI) equipped with a linear transducer (9L-D; GE Healthcare, Inc., Phoenix, AZ) operating at two different octave modes 2.4/4.8 MHz and 4/8 MHz. A suspension of CNF-stabilized PFC5 droplets (stock suspension diluted 10 times with Milli-Q water) was injected using a peristaltic pump (Watson-Marlow, Cornwall, UK) at a flow rate of  $35 \mu\text{L s}^{-1}$  to a tissue-mimicking Doppler flow phantom (Model 524, ATS Laboratories, Bridgeport, CT). The transducer was adjusted along the lumen of the channel perpendicular to the surface of the phantom. Ultrasound waves were focused on the lower part of the channel. At each mode, measurements were conducted in six independently fabricated samples to optimize the phase transition point. Real-time measurement and visualization were recorded at the stationary condition for the electrical attenuations between -24 and 0 dB (0.061 and 0.93 MPa as peak negative pressure) corresponding to a mechanical index (MI) from 0.02 to 1.2 at ultrasound frequency of 3.5 MHz. The attenuation was increased stepwise to monitor the increasing trend for the ultrasound wave and find out the pressure level at which phase transition occurred.

### 3. RESULTS AND DISCUSSION

#### 3.1. Preparation of CNF-Stabilized PFC Droplets.

Particle-stabilized PFC5 droplets were prepared in a straightforward manner by mixing cationic CNF with PFC5. The CNFs form a shell around the droplets suggesting a Pickering emulsion type of stabilization. Previous studies have emphasized the importance of nanocellulose with a low surface charge density in order to stabilize hydrocarbon oils such as hexadecane.<sup>27</sup> However, in the present study, due to the presence of electronegative fluorine atoms in PFC5, a cationic CNF was chosen. The expected electrostatic interactions between the positively charged quaternary ammonium groups on the CNF surface and the electronegative fluorine atoms in PFC5 most likely aided in the adsorption of CNFs at the O/W interface and thereby improved emulsion stability. In Figure 1a, an AFM image of the CNFs is presented, which shows CNFs with a width of ca. 4 nm and a length in the micrometer range.

As discussed in the introduction, a particular advantage with CNFs, is that micrometer-sized PFC5 droplet, in a comparatively narrow range (ca. 1–5 μm in size), can be achieved in a simple and straightforward way by merely mixing,<sup>26</sup> see Figure 1d as well as the discussion and results in the next section 3.2. The comparatively narrow size range and lower limit in droplet size is because CNFs consist of stiff

crystalline segments interconnected via more flexible amorphous regions. The size of the final droplets will, however, also depend on the amount of CNF used during preparation;<sup>18</sup> therefore, a high amount of CNF was used herein to achieve as small droplets as possible. The size of commercial ultrasound contrast agents is generally between 1 and 10  $\mu\text{m}$  in diameter, which is much larger than the cell spaces, and the present particle-stabilized droplets fits nicely within this size range.<sup>38</sup>

Another advantage with particle-stabilized droplets is that desorption energies for solid particles stabilizing an O/W interface are much higher than for surfactants, which makes particle-stabilized droplets remarkably stable.<sup>20</sup> Such particles can be thought of as being “irreversible” adsorbed at the interface. Stabilizing particles prevent the droplets from coalescing by creating a steric barrier at the interface (a high particle concentration at the interface further increases the stability), which enables increased shelf life.<sup>8,20</sup> Surfactants, on the other hand, are highly mobile and in dynamic equilibrium with the surfactants in the bulk and do not provide the same stability.<sup>8,39</sup> To prove that our CNFs can impart Pickering stabilization at the O/W interface, the complex viscoelastic modulus ( $E$ ) and interfacial tensions ( $\gamma$ ) were measured for an oscillating droplet of CNF suspension (0.28 wt %) in PFC5. The results from the DPT experiments are presented in Figure 2. The DPT technique can be used to quantify the accumulation of the CNF at the PFC5/water (oil/water) interface and also the stability of the created CNF-covered PFC5 droplets. The stability criterion, as formulated by Gibbs,<sup>20,40</sup> states that  $E$  should be equal to or exceed half the interfacial tension, i.e.  $E \geq \gamma/2$ . For the present system, the complex viscoelastic modulus increased with time, which shows that the accumulation of CNF at the O/W interface required some time to establish. Additionally, the interfacial tension decreased with time, see Figure 2a. The results show that, at long times ( $t \approx 60$  min), Gibb's stability criterion is achieved, showing that CNF is able to stabilize the PFC5/water interface, and the stability is achieved by a Pickering mechanism.<sup>21</sup> The results also showed that any formed CNF-stabilized PFC5 droplets will be stable enough at long times, which is advantageous from the point of view of storage stability. In Figure 2b, a SEM image of CNF-stabilized droplets is included, which shows that a coherent CNF-layer was indeed formed on top of the PFC5 droplets. The results in Figure 2a can also be compared to the results for a “naked” PFC5/water system, where the interface is not stabilized with particles. The reported interfacial tension at the PFC5/water interface in literature is  $56 \pm 1 \text{ mN m}^{-1}$ .<sup>15</sup> This value fits nicely with the obtained interfacial tension herein, which was  $\gamma = 53.2 \pm 0.5 \text{ mN m}^{-1}$ . The attained complex viscoelastic modulus was  $E = 4.8 \pm 3 \text{ mN m}^{-1}$  (both values are an average of two measurements), which gives  $E \ll \gamma/2$  for a “naked” PFC5 droplet in water. In this case, Gibb's stability criterion is not fulfilled, meaning that any formed PFC5 droplets in water will eventually merge into bigger droplets and the oil phase will coarsen and separate from the water phase.

**3.2. Effect of the Temperature Variation on CNF/PFC5 Droplets.** Acoustic droplet vaporization depends not only on the ultrasound parameters, such as ultrasound frequency and power, but also on temperature. To assess the feasibility of the present CNF-stabilized PFC5 droplets for the ultrasound-assisted vaporization, their behavior was studied by exposing them to the thermal variations. The size of droplets was investigated at different temperatures from 4 to 45 °C with

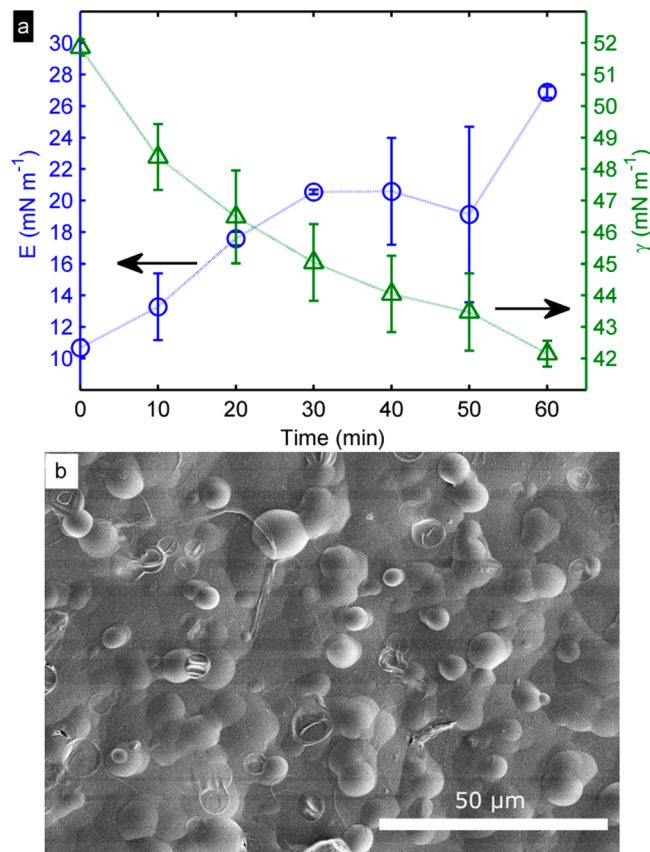


**Figure 2.** (a) DPT results. The complex viscoelastic modulus ( $E$ ) and interfacial tension ( $\gamma$ ) at the CNF-stabilized water/oil interface at different time points. The oscillation frequency was 0.3 Hz and measurements were performed at ambient conditions ( $T = 22$ ). The values are an average of two separate measurements. (b) SEM image of collapsed CNF-stabilized PFC5 droplets, where the PFC5 has evaporated. The left-over engraving CNF shell collapsed to different degrees.

5 °C increments at each step. The average diameter of the droplets at room temperature is approximately 3.5  $\mu\text{m}$  as shown in Figure 3b. The number of droplets was counted using a cell counter, which detects the number of droplets that have settled or are in the vicinity of the bottom of the measurement container. This was used as a first approximation to understand how many droplets were present in its liquid form, and thus heavier than water, at the different temperatures. In this way, we distinguish liquid droplets from liquid droplets converted to gas bubbles. Also, as larger droplets are also expected to settle faster at the bottom of the measurement container, the obtained sizes should not be confused with the average sizes for the entire samples, which would also require measurement of CNF-stabilized PFC5 droplets present in the bulk. The density of liquid PFC5 is 1.69 g  $\text{cm}^{-3}$  (1 atm), 1.63 g  $\text{cm}^{-3}$  (1 atm), and 1.578 g  $\text{cm}^{-3}$  (1.209 atm) at 4, 20, and 35 °C, respectively.<sup>41</sup>

As the temperature was decreased to 4 °C, the average size of the CNF-stabilized droplets decreased to approximately 3  $\mu\text{m}$ . The temperature decrease leads to an increased population of smaller droplets. Figure 3a shows that both mean and volume distributions reduced to ~3  $\mu\text{m}$  at 4 °C, which is due to the density increase of the encapsulated PFC5, and consequently droplet shrinkage, as the temperature decreased.

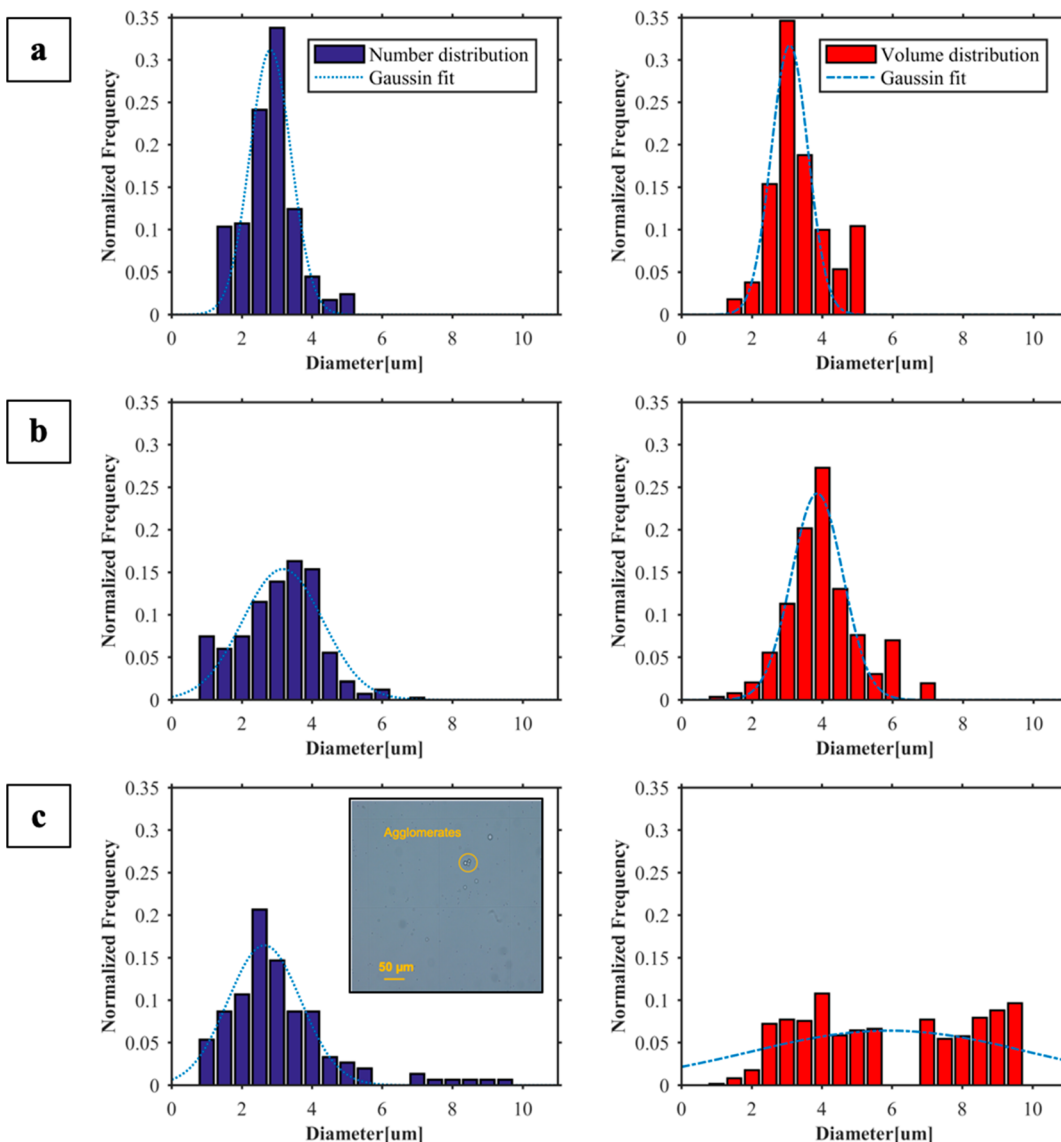


**Figure 3.** Normalized number and volume distributions for droplets at (a) 4 °C, (b) 20 °C, and (c) 45 °C on the bottom (or vicinity of the bottom) of the counting chamber.

The distribution in droplet size and volume was narrow, indicating the formation of tiny droplets with relatively small volume. The droplets return to their original size as the temperature was increased to the room temperature. Particular attention was paid to the size and volume distributions of the droplets at room temperature. The droplets in Figure 3b shows the regular view and distribution range of the CNF-stabilized PFC5 droplets at the room temperature where the magnitude of the droplets with moderate volumes (around 4  $\mu\text{m}$ ) was increased while there were considerable amounts of tiny droplets with a diameter of approximately 1  $\mu\text{m}$ . Note that 1  $\mu\text{m}$  is the lower detection limit in the analysis script.

As a result of the temperature increase to 45 °C (Figure 3c), bigger sizes were observed in addition to a decrease in the population of droplets. This observation is due to the fact that PFC5 droplets are converted from liquid to bubbles and migrate from the counting chamber bottom to the cover glass surface. This relocation happens due to the lower density of the bubbles (density of PFC5 gas is 0.012 g  $\text{cm}^{-3}$ ) in comparison to the water. Despite this, there still exists a

population of smaller liquid PFC5 droplets, with a maximum at around 2.5  $\mu\text{m}$  at the bottom of the counting chamber. It was also observed that, after the temperature of 45 °C, agglomerates were observed as illustrated in Figure 3c. The agglomerates extend the size to bigger values, around 10  $\mu\text{m}$  at higher temperatures. However, the agglomerates did not coalescence within the experimental time frame.

The PFC5 boiling point of 29.2 °C at the standard pressure of 1 atm is close to the room temperature. However, the present particle-stabilized droplets will experience an increased pressure inside the droplet ( $P_{\text{inside}}$ ), according to the Laplace pressure relationship:

$$\Delta P = P_{\text{inside}} - P_{\text{outside}} = 2\gamma/r \quad (2)$$

where  $\gamma$  is the interfacial tension and  $r$  is the radius of the droplets. The boiling point for the PFC inside the CNF-stabilized PFC droplets will be a function of the pressure and hence the size of the particle-stabilized droplet.<sup>15</sup>

$$\log_{10} P = A - \left( \frac{B}{T + C} \right) \quad (3)$$

With the use of the Antoine eq (eq 3) for the pressure dependence of the vaporization temperature, it is possible to deduct the droplet vaporization temperature as a function of the droplet size. The values of the A, B, and C parameters in the Antoine equation were reported in the study of Barber et al.<sup>42</sup> In Figure 4, the droplet-to-bubble transition temperature

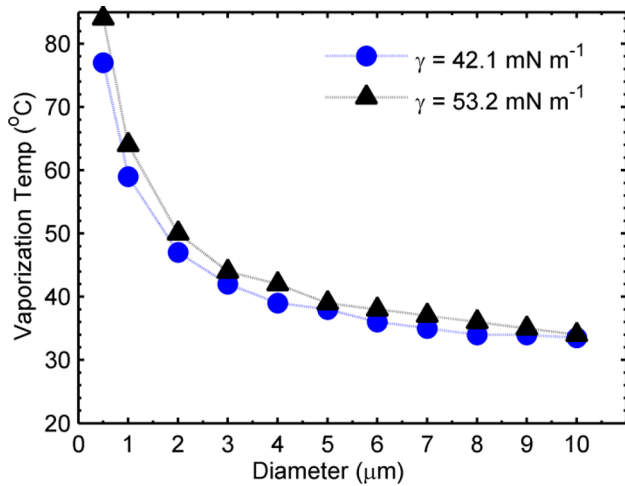


Figure 4. Droplet-to-bubble transition temperature (°C) as a function of droplet size (μm) for two different interfacial tensions ( $\gamma$ ).

is shown in the case of “naked” PFC5 droplets (using  $\gamma = 53.2 \text{ mN m}^{-1}$  in the calculations) and PFC5 droplets stabilized with CNF ( $\gamma = 42.1 \text{ mN m}^{-1}$ ).

In accordance with Figure 4, CNF-stabilized droplets smaller than ca.  $2.4 \mu\text{m}$  in diameter can only exist at temperatures around  $45^\circ\text{C}$ , which fits well with the experimental trend in Figure 3c (compare with results in Figure 3b).

In Figure 5, the volume fraction and concentration of the droplets as a function of temperature is presented. As illustrated in Figure 3, the population and size of the droplets reduce as the temperature increases from 4 to  $45^\circ\text{C}$ . Concentration and volume fraction have values at approximately 0.027 vol % and  $10^8 \text{ droplets mL}^{-1}$  below and at room temperature which could be explained by the fact that the liquid content inside the droplets and size distributions do not vary at the values below room temperature. The concentration

and volume fraction at the temperature of  $20^\circ\text{C}$  which is considered the room temperature in our experiments started to decrease due to nucleation from the boundaries and subcooling arrival. While both quantities presented a sharp decrease with increased temperature above the room temperature, with the arrival of bulk boiling point for the droplets at the temperature of approximately  $22^\circ\text{C}$ , the concentration and volume fraction shows a smoother decreasing trend implying the phase transition to gaseous microbubbles at  $29^\circ\text{C}$  and movement of the evaporated droplets to the glass cover due to the density difference. This trend is also observed in the deviations of the repeated test results, where the deviations at higher temperatures, over  $22^\circ\text{C}$ , are much smaller than at lower temperatures. The volume fraction and concentration values for the cooling part show an approximately constant trend prior to the arrival of the room temperature implying that there is no considerable transitions.

**3.3. Acoustic and Acoustophoresis Tests.** The crucial step of the ADV is the point where the droplet is entirely converted to the bubble. This stage can be described by the Keller–Miksits equation<sup>43</sup> where the classical Navier–Stokes equations together with the equation of state are considered. The instantaneous bubble radius and pressure inside the bubbles is assumed at the final moment of the droplet evolution. Apart from the droplet geometrical parameters and shell elasticity, the properties of the ultrasound waves, such as nonlinear distortion, play a significant role in the initial phase of the generated bubble and stability of the droplet activation pressure range.<sup>10</sup>

Figure 6 shows the phase transition steps for the CNF-stabilized PFC5 droplets at two different excitation frequencies 2.4 and 4 MHz. The droplets were introduced in the phantom at a regular flow rate, and the ultrasound wave was applied to the regions of interest (ROI) at the stationary condition, marked with circles of different colors in the ultrasound images of the tissue mimicking phantom. Two ROI:s (red and green circles inside the flow channel in the phantom) with the size covering the whole cross section of the tube were selected to follow the video intensity variations and sudden change corresponding to the phase transition of the droplet to bubble. Two ROI:s (yellow and blue) of the same size and shape were placed above and below the tube lumen (as references) to follow the video intensity during a stepwise electrical attenuation increase from  $-32$  to  $0 \text{ dB}$  ( $0.03$  and  $0.93 \text{ MPa}$  as peak negative pressure). As expected, at a low electrical attenuation ( $MI = 0.02, P_{\text{neg}} = 0.03 \text{ MPa}$ ), the video intensity

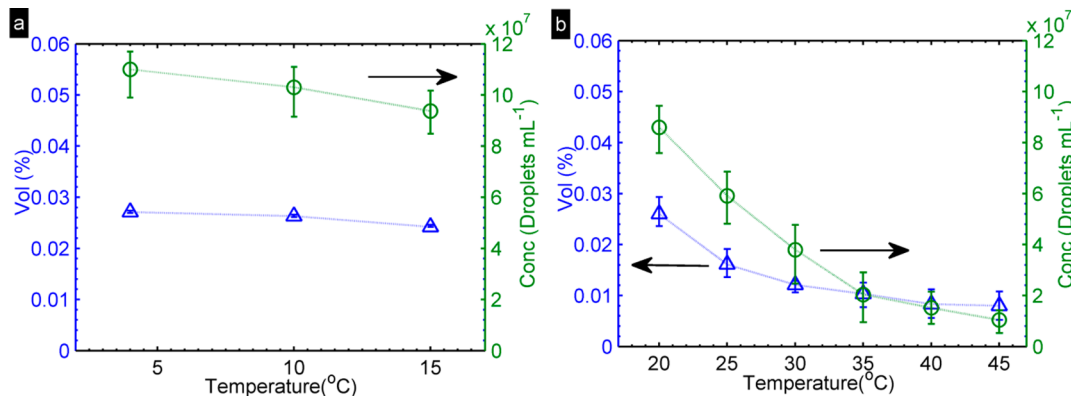
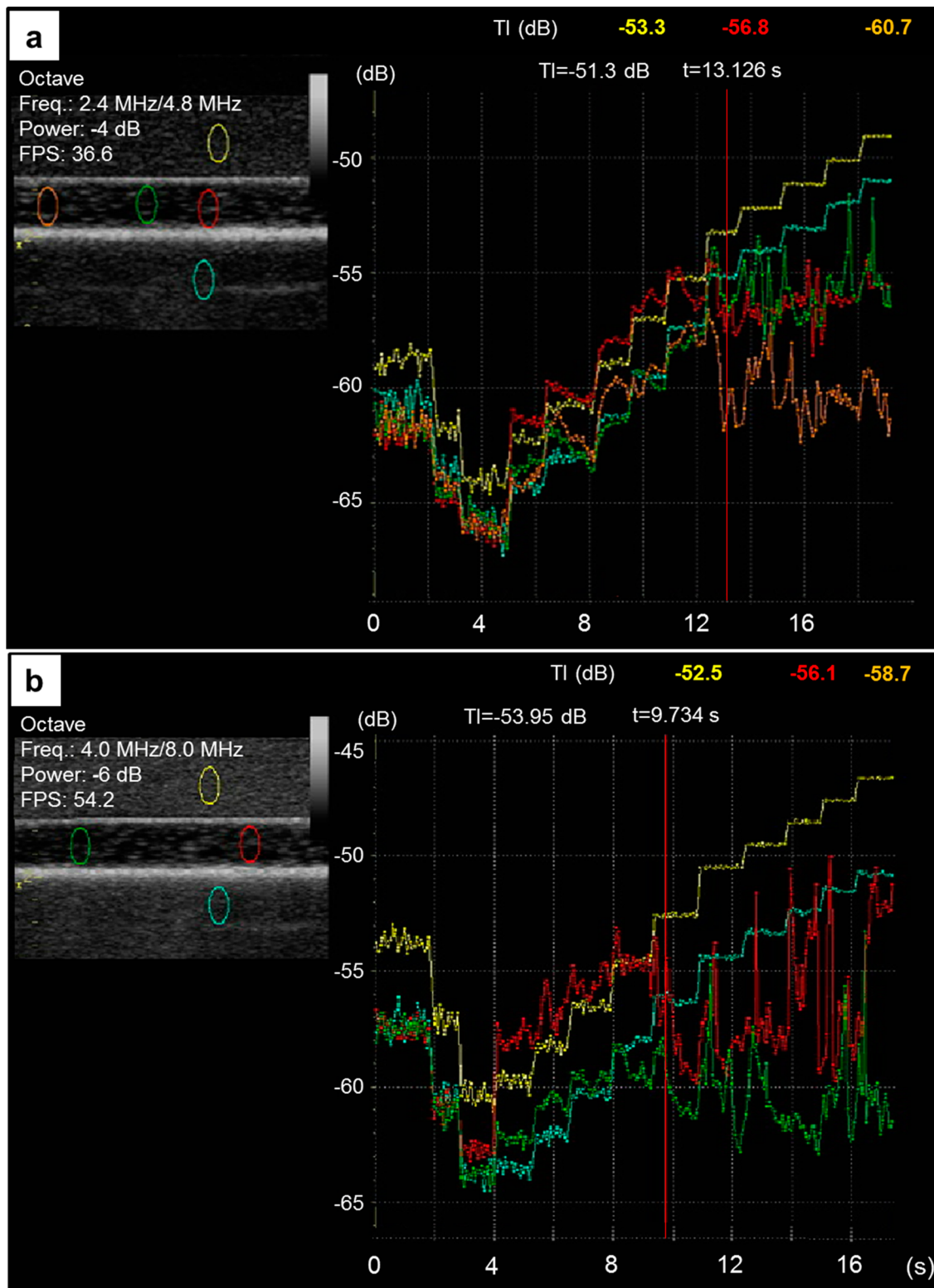


Figure 5. Volume fraction (vol, %) and concentration of the droplets (conc, droplets  $\text{mL}^{-1}$ ) exposed to (a) cooling and (b) heating.



**Figure 6.** Snapshots of acoustic tests. B-Mode ultrasound image acquired at octave mode with frequencies (a) freq: 2.4 MHz/4.8 MHz and (b) freq: 4 MHz/8 MHz. The plots include video intensity curves following a stepwise increase of electrical attenuation (in dB) during 16 s of recording (*x* axis). The curves were constructed from four to five regions of interest, marked with yellow, blue, green, orange, and red circles in the ultrasound images of a tissue-mimicking phantom (inset images). The yellow and blue regions are the phantom material (used as references), whereas the other regions are within the tubular cavity, through which the CNF-stabilized PFCS droplet suspension flows at a rate of  $35 \mu\text{L s}^{-1}$ . The red vertical lines in the plots mark the acoustic power at which droplets start converting to bubbles. The readers are also referred to [Movies S1](#) and [S2](#).

(see [Movies S1](#) and [S2](#)) increases linearly both for the solid tissue mimicking phantom and for CNF-stabilized droplets

with respect to the applied pressure, suggesting that droplets remain liquid-filled within the time of insonation. However, at

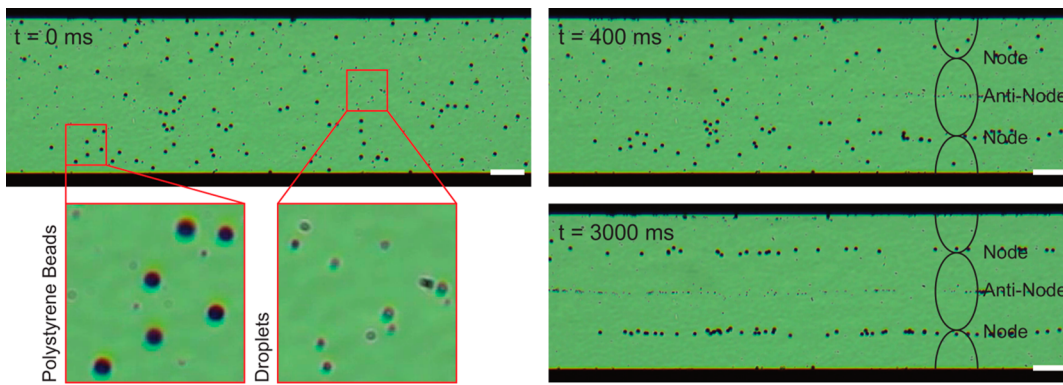


**Figure 7.** Droplets relocate to the pressure antinode and polystyrene beads relocate to the pressure nodes. A CNF/PFC5 droplet and 10  $\mu\text{m}$  polystyrene bead suspension (magnifications in inserts) are introduced into a 450  $\mu\text{m}$  wide silicon/glass microchannel and recorded during initial ultrasonic radiation force position manipulation. The images show video frames at different time points,  $t$ , and the stationary acoustic pressure field is schematically visualized to the right. The droplets and beads are in the same plane of focus. The scale bar is 100  $\mu\text{m}$  in all images.

( $\text{MI} = 0.4$ ,  $P_{\text{neg}} = 0.62 \text{ MPa}$ ), the video intensity starts to fluctuate and flicker with each following insonation period. These points are marked with vertical red lines in the plots in Figure 6. The sudden changes in the consecutive peak values of the video intensity suggest the significant changes in the media corresponding to the phase transition of droplets to bubbles.

The behavior of single perfluoropentane droplets exposed to the ultrasonic waves induced by a transducer at different frequencies has been studied previously.<sup>44</sup> Furthermore, it is reported that the incident nucleation pressure is much lower than the pressure inducing bubble collapse and condensation.<sup>9</sup> These studies imply the significant role of the applied frequency regarding droplet phase shift and subsequent mechanisms as a result of the acoustic wave exposure. The recent studies also show that the acoustic pressure threshold for the nucleation is inversely proportional to the size of the droplets.<sup>45</sup>

In general, microbubbles (MBs) with different shell thicknesses can be utilized as an independent drug delivery system due to differences in mechanical stability. It was shown that while the thin-shelled MBs have a buckling response to the ultrasound pressure at low magnitudes, the thicker ones have instant destructive behavior, violent gas evacuation, and dissipation at activation pressures above the threshold.<sup>46</sup> This might hinder currently available ultrasound contrast agents as a tool in modern theranostic applications. In the current study, the ADV event is further confirmed by the fact that gas-filled bubbles while oscillating in a nonlinear fashion will emit the acoustic signal at higher harmonics and will be detected by an ultrasound system operated in octave mode, i.e. harmonic imaging, used in this study. As illustrated in Figure 6b, with increasing the excitation frequency from 2.4 to 4 MHz the ADV occurs at the higher peak negative pressure [ $\text{MI} = 0.5$   $P_{\text{neg}} = 1 \text{ MPa}$  (for 4 MHz);  $P_{\text{neg}} = 0.62 \text{ MPa}$  (for 2.4 MHz)] and more sudden and dramatic changes between each image frame were observed. The latter suggests that, at a maximum power delivered from the system ( $\text{MI} = 0.6$ ,  $\text{TI} = 0.2$ ,  $P_{\text{neg}} = 1.2 \text{ MPa}$ ), we might visualize not only ADV but also the cavitation and collapse of the resulting microbubbles.

To further understand the particle-stabilized PFC5 droplet characteristics, a diluted CNF/PFC5 droplet and 10  $\mu\text{m}$  polystyrene bead suspension were introduced in a temperature-controlled silicon/glass microfluidic channel, mounted in a camera-equipped microscope, prior to ultrasonic standing

wave (USW) actuation, see Figure 7. The temperature was regulated around 15 °C to decouple possible temperature-dependent ADV from USW-induced ADV. The CNF/PFC5 droplets sedimented to the channel bottom, which was confirmed by visually verifying that they were in the same focal plane as the polystyrene beads, see lower left part of panel in Figure 7. When the ultrasound was turned on, the droplets were manipulated into the pressure antinodes along the channel (Figure 7, right part) and the 10  $\mu\text{m}$  polystyrene beads were, as expected to theory, focused to the pressure node. The acoustic pressure amplitude in the channel was estimated to  $0.16 \pm 0.04 \text{ MPa}$  by tracking 57 polystyrene beads during initial focusing and fit their trajectory velocities to the acoustic pressure. The droplet trapping into the pressure antinodes indicated a negative acoustic contrast factor of the droplets compared to the surrounding water. The acoustic contrast factor depends on the density and compressibility differences between a small particle and the surrounding wave carrying medium.<sup>47</sup> The CNF/PFC5 droplet density is higher than water at 15 °C since the droplets sediment to the channel bottom, and therefore, the negative acoustic contrast factor is due to the higher compressibility of the droplet compared to water. A positive contrast factor would have resulted in droplets being trapped in the pressure nodes together with the polystyrene beads which have both higher density and lower compressibility compared to the surrounding water.<sup>35</sup> Hence, even though droplets are liquid-filled and heavier than water, with basically similar properties as red blood cells or other types of human cells, the droplets relocate to another place (pressure antinode instead of node as for the cells). This opens up the possibility to separate cells and droplets, thereby providing knowledge of interaction between those two compounds.<sup>48</sup> This is a first step toward developing not only localized but also rather targeted and specific drug delivery if antibodies will be attached to the surface of the droplets.

## CONCLUSIONS

A novel class of PFC5 droplets stabilized with cationic cellulose nanofibers (CNFs) has successfully been prepared. DPT results confirmed that the PFC5/water interface was stabilized via a Pickering mechanism. The sizes of the attained droplets, ca. 1–5  $\mu\text{m}$ , were in the right size range for acoustic applications (100 nm–10  $\mu\text{m}$ ). However, only a simple and straightforward mixing protocol was necessary to achieve these

sizes, which makes CNFs an interesting material in ultrasound contrast-agent fabrication. Two major mechanisms: thermal and acoustic, which affect droplet vaporization, were individually investigated at a broad range of temperatures (4 to 45 °C) and peak negative pressures (0 to 1.2 MPa). The study reveals a vaporization temperature threshold at 22 °C where primarily larger droplets, above ca. 3 μm in diameter, were converted into bubbles, whereas a larger fraction of the smaller droplet population could withstand higher temperatures. Acoustic pressure thresholds of 0.62 MPa at 2.4 MHz and 1 MPa when the frequency was increased to 4 MHz, were identified using the clinical ultrasound machine operated in harmonic imaging mode.

Ultrasound standing wave experiments performed at 0.16 MPa, which is below vaporization pressure threshold, demonstrated that liquid-filled droplets behave as the negative contrast particles and form clusters at the antinodes, which is an unexpected result considering their high density, but due to the higher compressibility of the droplet compared to water. We are presently investigating the compressibility and density of the PFCS droplets from the experimental point of view using microfluidic systems. This property makes the CNF-stabilized PFCS droplets interesting in cell sortation and cell-droplet interaction experiments in microfluidics channels. Also, as CNF are rich in hydroxyl groups, it is possible to further modify the surface, potentially rendering present systems suitable for, e.g., combined targeted drug delivery and ultrasound imaging.

## ■ ASSOCIATED CONTENT

### Supporting Information

The Supporting Information is available free of charge on the ACS Publications website at DOI: [10.1021/acs.langmuir.9b02132](https://doi.org/10.1021/acs.langmuir.9b02132).

Movie S1 shows a B-mode ultrasound acquired at octave mode with frequencies of Freq: 2.4 MHz/4.8 MHz, following stepwise increase of electrical attenuation during 16 s of recording ([AVI](#))

Movie S2 shows a B-mode ultrasound acquired at octave mode with frequencies of Freq: 4 MHz/8 MHz, following stepwise increase of electrical attenuation during 16 s of recording ([AVI](#))

## ■ AUTHOR INFORMATION

### Corresponding Author

\*E-mail: [svagan@kth.se](mailto:svagan@kth.se).

### ORCID

Thomas Paulraj: [0000-0001-5098-3525](https://orcid.org/0000-0001-5098-3525)

Anna J. Svagan: [0000-0002-4583-723X](https://orcid.org/0000-0002-4583-723X)

### Notes

The authors declare no competing financial interest.

## ■ ACKNOWLEDGMENTS

A.J.S. would like to acknowledge the KTH starting grant for financial support.

## ■ REFERENCES

- (1) Samuel, S.; Duprey, A.; Fabiilli, M. L.; Bull, J. L.; Brian Fowlkes, J. In Vivo Microscopy of Targeted Vessel Occlusion Employing Acoustic Droplet Vaporization. *Microcirculation* **2012**, *19* (6), 501–509.
- (2) Zhu, M.; Jiang, L.; Fabiilli, M. L.; Zhang, A.; Fowlkes, J. B.; Xu, L. X Treatment of murine tumors using acoustic droplet vaporization-enhanced high intensity focused ultrasound. *Phys. Med. Biol.* **2013**, *58* (17), 6179.
- (3) Kang, S.-T.; Yeh, C.-K. Intracellular Acoustic Droplet Vaporization in a Single Peritoneal Macrophage for Drug Delivery Applications. *Langmuir* **2011**, *27* (21), 13183–13188.
- (4) Zhang, M.; Fabiilli, M. L.; Haworth, K. J.; Padilla, F.; Swanson, S. D.; Kripfgans, O. D.; Carson, P. L.; Fowlkes, J. B. Acoustic Droplet Vaporization for Enhancement of Thermal Ablation by High Intensity Focused Ultrasound. *Academic Radiology* **2011**, *18* (9), 1123–1132.
- (5) Arena, C. B.; Novell, A.; Sheeran, P. S.; Puett, C.; Moyer, L. C.; Dayton, P. A. Dual-frequency acoustic droplet vaporization detection for medical imaging. *IEEE Transactions on Ultrasonics, Ferroelectrics, and Frequency Control* **2015**, *62* (9), 1623–1633.
- (6) Kripfgans, O. D.; Fowlkes, J. B.; Miller, D. L.; Eldevik, O. P.; Carson, P. L. Acoustic droplet vaporization for therapeutic and diagnostic applications. *Ultrasound in Medicine & Biology* **2000**, *26* (7), 1177–1189.
- (7) Qamar, A.; Wong, Z. Z.; Fowlkes, J. B.; Bull, J. L. Dynamics of acoustic droplet vaporization in gas embolotherapy. *Appl. Phys. Lett.* **2010**, *96* (14), 143702–143702.
- (8) Lam, S.; Velikov, K. P.; Velev, O. D. Pickering stabilization of foams and emulsions with particles of biological origin. *Curr. Opin. Colloid Interface Sci.* **2014**, *19* (5), 490–500.
- (9) Seda, R.; Harmon, J.; Fowlkes, J. B.; Bull, J. Use of pulse repetition frequency to augment acoustic droplet vaporization in vivo. *J. Acoust. Soc. Am.* **2016**, *140* (4), 3026–3026.
- (10) Williams, R.; Wright, C.; Cherin, E.; Reznik, N.; Lee, M.; Gorelikov, I.; Foster, F. S.; Matsuura, N.; Burns, P. N. Characterization of Submicron Phase-change Perfluorocarbon Droplets for Extravascular Ultrasound Imaging of Cancer. *Ultrasound in Medicine & Biology* **2013**, *39* (3), 475–489.
- (11) Ho, Y.-J.; Chang, Y.-C.; Yeh, C.-K. Improving Nanoparticle Penetration in Tumors by Vascular Disruption with Acoustic Droplet Vaporization. *Theranostics* **2016**, *6* (3), 392–403.
- (12) Sakata, M.; Kazama, H.; Miki, A.; Yoshida, A.; Haga, M.; Morita, M. Acute toxicity of fluorocarbon-22: Toxic symptoms, lethal concentration, and its fate in rabbit and mouse. *Toxicol. Appl. Pharmacol.* **1981**, *59* (1), 64–70.
- (13) Song, X.; Feng, L.; Liang, C.; Yang, K.; Liu, Z. Ultrasound Triggered Tumor Oxygenation with Oxygen-Shuttle Nanoperfluorocarbon to Overcome Hypoxia-Associated Resistance in Cancer Therapies. *Nano Lett.* **2016**, *16* (10), 6145–6153.
- (14) Phillips, L. C.; Puett, C.; Sheeran, P. S.; Dayton, P. A.; Wilson Miller, G.; Matsunaga, T. O. Phase-shift perfluorocarbon agents enhance high intensity focused ultrasound thermal delivery with reduced near-field heating. *J. Acoust. Soc. Am.* **2013**, *134* (2), 1473–1473.
- (15) Rapoport, N.; Nam, K.-H.; Gupta, R.; Gao, Z.; Mohan, P.; Payne, A.; Todd, N.; Liu, X.; Kim, T.; Shea, J.; Scaife, C.; Parker, D. L.; Jeong, E.-K.; Kennedy, A. M. Ultrasound-mediated tumor imaging and nanotherapy using drug loaded, block copolymer stabilized perfluorocarbon nanoemulsions. *J. Controlled Release* **2011**, *153* (1), 4–15.
- (16) Aliabouzar, M.; Kumar, K. N.; Sarkar, K. Acoustic vaporization threshold of lipid-coated perfluoropentane droplets. *J. Acoust. Soc. Am.* **2018**, *143* (4), 2001–2012.
- (17) Capece, S.; Chiessi, E.; Cavalli, R.; Giustetto, P.; Grishenkov, D.; Paradossi, G. A general strategy for obtaining biodegradable polymer shelled microbubbles as theranostic devices. *Chem. Commun.* **2013**, *49* (51), 5763–5765.
- (18) Kalashnikova, I.; Bizot, H.; Cathala, B.; Capron, I. New Pickering Emulsions Stabilized by Bacterial Cellulose Nanocrystals. *Langmuir* **2011**, *27* (12), 7471–7479.
- (19) Bizmark, N.; Ioannidis, M. A. Ethyl Cellulose Nanoparticles at the Alkane-Water Interface and the Making of Pickering Emulsions. *Langmuir* **2017**, *33* (40), 10568–10576.

- (20) Stocco, A.; Drenckhan, W.; Rio, E.; Langevin, D.; Binks, B. P. Particle-stabilised foams: an interfacial study. *Soft Matter* **2009**, *5* (11), 2215–2222.
- (21) Pickering, S. U. CXCVI.—Emulsions. *J. Chem. Soc., Trans.* **1907**, *91* (0), 2001–2021.
- (22) Reznik, N.; Seo, M.; Williams, R.; Bolewski-Pedyczak, E.; Lee, M.; Matsuura, N.; Gariepy, J.; Foster, F. S.; Burns, P. N Optical studies of vaporization and stability of fluorescently labelled perfluorocarbon droplets. *Phys. Med. Biol.* **2012**, *57* (21), 7205.
- (23) Hannah, A.; Luke, G.; Wilson, K.; Homan, K.; Emelianov, S. Indocyanine Green-Loaded Photoacoustic Nanodroplets: Dual Contrast Nanoconstructs for Enhanced Photoacoustic and Ultrasound Imaging. *ACS Nano* **2014**, *8* (1), 250–259.
- (24) Niu, C.; Wang, L.; Wang, Z.; Xu, Y.; Hu, Y.; Peng, Q. Laser irradiated fluorescent perfluorocarbon microparticles in 2-D and 3-D breast cancer cell models. *Sci. Rep.* **2017**, *7*, 43408.
- (25) Nordenstrom, M.; Riazanova, A. V.; Jarn, M.; Paulraj, T.; Turner, C.; Strom, V.; Olsson, R. T.; Svagan, A. J. Superamphiphobic coatings based on liquid-core microcapsules with engineered capsule walls and functionality. *Sci. Rep.* **2018**, *8*, 1 DOI: [10.1038/s41598-018-21957-y](https://doi.org/10.1038/s41598-018-21957-y).
- (26) Svagan, A. J.; Musyanovich, A.; Kappl, M.; Bernhardt, M.; Glasser, G.; Wohnhaas, C.; Berglund, L. A.; Risbo, J.; Landfester, K. Cellulose Nanofiber/Nanocrystal Reinforced Capsules: A Fast and Facile Approach Toward Assembly of Liquid-Core Capsules with High Mechanical Stability. *Biomacromolecules* **2014**, *15* (5), 1852–1859.
- (27) Kalashnikova, I.; Bizot, H.; Cathala, B.; Capron, I. Modulation of Cellulose Nanocrystals Amphiphilic Properties to Stabilize Oil/Water Interface. *Biomacromolecules* **2012**, *13* (1), 267–275.
- (28) Fujisawa, S.; Togawa, E.; Kuroda, K. Facile Route to Transparent, Strong, and Thermally Stable Nanocellulose/Polymer Nanocomposites from an Aqueous Pickering Emulsion. *Biomacromolecules* **2017**, *18* (1), 266–271.
- (29) Xu, H.-N.; Li, Y.-H.; Zhang, L. Driving Forces for Accumulation of Cellulose Nanofibrils at the Oil/Water Interface. *Langmuir* **2018**, *34* (36), 10757–10763.
- (30) Bai, L.; Huan, S.; Xiang, W.; Rojas, O. J. Pickering emulsions by combining cellulose nanofibrils and nanocrystals: phase behavior and depletion stabilization. *Green Chem.* **2018**, *20* (7), 1571–1582.
- (31) Tang, C.; Spinney, S.; Shi, Z.; Tang, J.; Peng, B.; Luo, J.; Tam, K. C. Amphiphilic Cellulose Nanocrystals for Enhanced Pickering Emulsion Stabilization. *Langmuir* **2018**, *34* (43), 12897–12905.
- (32) Svagan, A. J.; Benjamins, J.-W.; Al-Ansari, Z.; Shalom, D. B.; Müllertz, A.; Wåberg, L.; Löbmann, K. Solid cellulose nanofiber based foams - Towards facile design of sustained drug delivery systems. *J. Controlled Release* **2016**, *244*, 74–82.
- (33) Ohlin, M.; Iranmanesh, I.; Christakou, A. E.; Wiklund, M. Temperature-controlled MPa-pressure ultrasonic cell manipulation in a microfluidic chip. *Lab Chip* **2015**, *15* (16), 3341–9.
- (34) Christakou, A. E.; Ohlin, M.; Önfelt, B.; Wiklund, M. Ultrasonic three-dimensional on-chip cell culture for dynamic studies of tumor immune surveillance by natural killer cells. *Lab Chip* **2015**, *15* (15), 3222–3231.
- (35) Vanherberghen, B.; Manneberg, O.; Christakou, A.; Frisk, T.; Ohlin, M.; Hertz, H. M.; Önfelt, B.; Wiklund, M. Ultrasound-controlled cell aggregation in a multi-well chip. *Lab Chip* **2010**, *10* (20), 2727–2732.
- (36) Tinevez, J. Y.; Perry, N.; Schindelin, J.; Hoopes, G. M.; Reynolds, G. D.; Laplantine, E.; Bednarek, S. Y.; Shorte, S. L.; Eliceiri, K. W. TrackMate: An open and extensible platform for single-particle tracking. *Methods* **2017**, *115*, 80.
- (37) Bruus, H. Acoustofluidics 7: The acoustic radiation force on small particles. *Lab Chip* **2012**, *12* (6), 1014–21.
- (38) Mullin, L.; Gessner, R.; Kwan, J.; Kaya, M.; Borden, M. A.; Dayton, P. A. Effect of anesthesia carrier gas on in vivo circulation times of ultrasound microbubble contrast agents in rats. *Contrast Media Mol. Imaging* **2011**, *6* (3), 126–131.
- (39) Chevalier, Y.; Bolzinger, M.-A. Emulsions stabilized with solid nanoparticles: Pickering emulsions. *Colloids Surf., A* **2013**, *439*, 23–34.
- (40) Bannow, J.; Benjamins, J. W.; Wohlt, J.; Lobmann, K.; Svagan, A. J. Solid nanofoams based on cellulose nanofibers and indomethacin—the effect of processing parameters and drug content on material structure. *Int. J. Pharm.* **2017**, *526* (1–2), 291–299.
- (41) Lindstrom, P. J.; Mallard, W. G. *NIST Chemistry Web Book, NIST Standard Reference Database*, 69th ed.; NIST, 2018.
- (42) Barber, E. J.; Cady, G. H. Vapor Pressures of Perfluoropentanes. *J. Phys. Chem.* **1956**, *60* (4), 504–505.
- (43) Keller, J. B.; Miksis, M. Bubble Oscillations of Large-Amplitude. *J. Acoust. Soc. Am.* **1980**, *68* (2), 628–633.
- (44) Miles, C. J.; Doering, C. R.; Kripfgans, O. D. Nucleation pressure threshold in acoustic droplet vaporization. *J. Appl. Phys.* **2016**, *120* (3), 034903.
- (45) Kripfgans, O. D.; Fabiilli, M. L.; Carson, P. L.; Fowlkes, J. B. On the acoustic vaporization of micrometer-sized droplets. *J. Acoust. Soc. Am.* **2004**, *116* (1), 272–281.
- (46) Lensen, D.; Gelderblom, E. C.; Vriezema, D. M.; Marmottant, P.; Verdonschot, N.; Versluis, M.; de Jong, N.; van Hest, J. C. M. Biodegradable polymeric microcapsules for selective ultrasound-triggered drug release. *Soft Matter* **2011**, *7* (11), 5417–5422.
- (47) Bruus, H. Acoustofluidics 7: The acoustic radiation force on small particles. *Lab Chip* **2012**, *12* (6), 1014–1021.
- (48) Faridi, M. A.; Ramachandraiah, H.; Iranmanesh, I.; Grishenkov, D.; Wiklund, M.; Russom, A. MicroBubble activated acoustic cell sorting. *Biomed. Microdevices* **2017**, *19* (2), 23.